remote sensing

MDPI

Article

Large-Scale Urban Heating and Pollution Domes over the Indian Subcontinent

Trisha Chakraborty [1], Debashish Das [2], Rafiq Hamdi [3], Ansar Khan [4,*] and Dev Niyogi [5,6]

[1] School of Environmental Studies, Jadavpur University, Kolkata 700032, India; trishac.sest.rs@jadavpuruniversity.in
[2] Department of Architecture, Jadavpur University, Kolkata 700032, India; ddasju.arch@jadavpuruniversity.in
[3] Royal Meteorological Institute of Belgium, 1180 Bruxelles, Belgium; rafiq.hamdi@meteo.be
[4] Department of Geography, Lalbaba College, University of Calcutta, Howrah 711201, India
[5] Department of Geological (Earth and Planetary) Sciences, Jackson School of Geosciences, The University of Texas at Austin, Austin, TX 78759, USA; dev.niyogi@jsg.utexas.edu
[6] Department of Civil, Architectural, and Environmental Engineering, Cockrell School of Engineering, The University of Texas at Austin, Austin, TX 78759, USA
* Correspondence: ansar.geog@lalbabacollege.in

Abstract: The unique geographical diversity and rapid urbanization across the Indian subcontinent give rise to large-scale spatiotemporal variations in urban heating and air emissions. The complex relationship between geophysical parameters and anthropogenic activity is vital in understanding the urban environment. This study analyses the characteristics of heating events using aerosol optical depth (AOD) level variability, across 43 urban agglomerations (UAs) with populations of a million or more, along with 13 industrial districts (IDs), and 14 biosphere reserves (BRs) in the Indian sub-continent. Pre-monsoon average surface heating was highest in the urban areas of the western (42 °C), central (41.9 °C), and southern parts (40 °C) of the Indian subcontinent. High concentration of AOD in the eastern part of the Indo-Gangetic Plain including the megacity: Kolkata (decadal average 0.708) was noted relative to other UAs over time. The statistically significant negative correlation (−0.51) between land surface temperature (LST) and AOD in urban areas during pre-monsoon time illustrates how aerosol loading impacts the surface radiation and has a net effect of reducing surface temperatures. Notable interannual variability was noted with, the pre-monsoon LST dropping in 2020 across most of the selected urban regions (approx. 89% urban clusters) while it was high in 2019 (for approx. 92% urban clusters) in the pre-monsoon season. The results indicate complex variability and correlations between LST and urban aerosol at large scales across the Indian subcontinent. These large-scale observations suggest a need for more in-depth analysis at city scales to understand the interplay and combined variability between physical and anthropogenic atmospheric parameters in mesoscale and microscale climates.

Keywords: land surface temperature; aerosol optical depth; urban agglomeration; industrial districts; biosphere reserve

Citation: Chakraborty, T.; Das, D.; Hamdi, R.; Khan, A.; Niyogi, D. Large-Scale Urban Heating and Pollution Domes over the Indian Subcontinent. *Remote Sens.* **2023**, *15*, 2681. https://doi.org/10.3390/rs15102681

Academic Editor: Weiqi Zhou

Received: 23 March 2023
Revised: 17 May 2023
Accepted: 19 May 2023
Published: 22 May 2023

1. Introduction

Urbanization and industrialization have led to a rise in pollution levels and increased urban heating. The widespread urbanization likely leads to a large-scale scenario of urban heating and pollution domes over the Indian subcontinent. Such pollutant loading can have significant impacts on the environment and public health. Urban environments and dwellers are heterogeneously impacted by different types of air pollution and urban heating. This, inequity emphasizes the need for researching the impacts of urban pollution islands (UPIs) and urban heat islands (UHIs) on local and regional scales [1]. The Indian subcontinent, where 18.1% of the world's population resides, was responsible for 26.2% of the disability-adjusted life years caused by air pollution in the world in 2017 [2]. Assessing

these issues requires a multi-faceted approach, including reducing emissions from vehicles and industrial activity, increasing green space and urban forestry, and promoting public transportation and sustainable urban planning.

During the pre-monsoon season, urban meteorological processes across the Indian subcontinent due to lack of active rain events have a considerable impact on aerosol optical depth (AOD) and air pollution loading, thereby affecting air quality [3]. In this study, AOD, a unitless quantity, which quantifies the total amount of solar radiation absorbed or scattered by particles suspended in the atmosphere at specific wavelengths is used as a measure of aerosol loading [4]. Aerosols alter the surface-atmosphere energy budget by directly reducing solar irradiance through absorption and scattering, altering the tropospheric temperatures, and regionally warming or cooling the earth's surface temperature [5–9].

Anthropogenic aerosols from southern and eastern Asia are mainly found in an air mass extending from the Indian Ocean to the North Pacific Ocean. The aerosol-induced surface temperature changes have an impact on a local to global scale [10]. A notable dust source region in southern Asia disperses the dust to form a crescent-shaped dust plume extending from the Thar Desert to the Indo-Gangetic Plain in India. The pre-monsoon (March, April, and May) period is the peak period for such dust transport. Mineral dust transported from Africa, Arabia, and the Thar Desert as well as crop residue burning in northwest India are often the main causes of the dust optical depth (DOD) over the entire Indo-Gangetic plain [11–13]. The Indo-Gangetic Plain (IGP) in Southern Asia is a global hot spot with unremitting high AOD as routinely monitored by a variety of satellite remote sensors (MODIS, MISR, SeaWiFS), and ground-based sensors (AERONET) [14]. The relationship between AOD and surface temperature was negative for both seasons (winter & summer) over north-eastern India and the western coastal area around Mumbai [15].

The unique topography of the Indian subcontinent, particularly the Himalayan region in the north and the Thar Desert in the west, is primarily responsible for its temperature variation patterns [15]. Nearly all the climate zones in northwest, central, and western India, as well as some subdivisions in the south, have experienced high temperatures and an increasing number of hot days during the pre-monsoon period from March to May [16]. Climatologically, western and southern regions experience the warmest temperatures in April, while northern regions experience the warmest temperatures in May [17].

A city's near-surface air temperatures and land surface temperatures are of primary interest in studying how anthropogenic activities interact with the urban environment and urban climate and in observing how urbanization affects the environment. Studies examining the surface urban heat island (SUHI) effect are based mainly on land surface temperature (LST) estimates. LST is a prominent geophysical variable that can be estimated remotely by satellite sensors (MODIS, AVHRR, etc.). It has been used in several SUHI-related applications, including the estimation of surface fluxes and energy budgets [18,19].

In this study, LST and AOD were studied during the pre-monsoon (March–May) to observe spatiotemporal variations in urban areas and biosphere reserves. An understanding of the relationship between AOD and LST was also sought in different geophysical environments across the Indian subcontinent. Worldwide, several studies show a negative relationship between LST and AOD, while some show a positive one [20–26]. Increasing AOD levels affect the earth's energy budget by scattering and absorbing insolation. As a result, the land surface may be cooled [23]. Based on a study conducted in Delhi in 2007 and 2008, high levels of AOD tend to have lower surface temperatures during daytime [20]. Researchers also have found that in urban centers of Berlin, incoming solar radiation was reduced due to increased aerosols in the atmosphere (2010–2017), and the outgoing longwave radiation also increased with the aerosol levels in the atmosphere. With a correlation coefficient of −0.31, the AOD shows a negative association with the LST, especially at night when the longwave radiation is more significant [21]. Similar results have been observed in Bengaluru including a negative correlation between urban and non-urban LST and AOD. It was also found that AOD increased significantly in winter [22]. Most of the

studies over the Indian subcontinent related to AOD and LST are in the Indo-Gangetic Plain. A two-decade long analysis over the Ganga River Basin (2001–2019), showed LST is negatively correlated with AOD. Incoming solar radiation is more likely to be absorbed by aerosols [26]. In contrast, a similar two-decade long analysis of data over Dhaka showed a positive correlation between AOD and LST (1999–2019) [25]. Elsewhere, across the entire boreal region, no clear relationship between AOD and LST has been observed [27]. This follows that AOD and LST have a complex relationship that is a function of the location, season, and time of day. There is a gap in the literature due to the absence of a comparison between the previously mentioned relationship in forests and urban areas. Therefore, it is important to consider different geophysical settings of the Indian subcontinent to observe the relation between the parameters.

2. Materials and Methods

In this study over the Indian region, 43 urban agglomerations (UAs) (Table 1) and 13 industrial districts (IDs) (Table 2) were initially identified to study the relationship between geophysical parameters and their effects on the urban climate. As per the 2021 census, an urban agglomeration is a densely populated, continuously growing urban area with a combined effect of two or more physically adjacent towns and their outgrowths (OGs) or of two or more outgrowths of those towns. From the 2011 Census, an UA must include at least one statutory town with a total population of at least 20,000 [28].

Table 1. Population data of urban agglomerations (UAs) according to the 2011 census.

Code	Urban Agglomeration	Population	Code	Urban Agglomeration	Population
UA1	Kolkata	14,112,536	UA23	Surat	4,585,367
UA2	Asansol	1,243,008	UA24	Vadodara	1,817,191
UA3	Dhanbad	1,195,298	UA25	Rajkot	1,390,933
UA4	Ranchi	1,126,741	UA26	Mumbai	18,414,288
UA5	Jamshedpur	1,337,131	UA27	Pune	5,049,968
UA6	Patna	2,046,652	UA28	Nashik	1,562,769
UA7	Lucknow	2,901,474	UA29	Raipur	1,122,555
UA8	Kanpur	2,920,067	UA30	Durg-Bhilainagar	1,064,077
UA9	Allahabad	1,216,719	UA31	Hyderabad	7,749,334
UA10	Varanasi	1,435,113	UA32	Vijayawada	1,491,202
UA11	Meerut	1,424,908	UA33	Bangalore	8,499,399
UA12	Ghaziabad	2,358,525	UA34	Chennai	8,696,010
UA13	Agra	1,746,467	UA35	Coimbatore	2,151,466
UA14	Delhi	16,314,838	UA36	Madurai	1,462,420
UA15	Chandigarh	1,025,682	UA37	Kannur	1,642,892
UA16	Amritsar	1,183,705	UA38	Kozhikode	2,030,519
UA17	Jodhpur	1,137,815	UA39	Kollam	1,110,005
UA18	Gwalior	1,101,981	UA40	Thiruvanantapuram	1,687,406
UA19	Bhopal	1,883,381	UA41	Thrissur	1,854,783
UA20	Indore	2,167,447	UA42	Kochi	2,117,990
UA21	Jabalpur	1,267,564	UA43	Malappuram	1,698,645
UA22	Ahmedabad	6,352,254			

The 13 industrial districts refer to a geographic concentration of small and medium enterprises (SMEs) and some large firms in the same or related industries that are in close proximity to each other. These districts are characterized by a strong emphasis on local entrepreneurship and are highly specialized in several stages of the process and actively involved in producing a specific product or group of products through a dense network of inter-firm cooperative and competitive relationships [29]. In India, the Ministry of Micro, Small and Medium Enterprises (MSME) have implemented The Cluster Development Program, which provides financial and technical support to clusters of industries [30].

Table 2. Population data of industrial districts (IDs) according to the 2011 census.

Code	Industrial Districts	Population
ID1	Jalpaiguri	107,351
ID2	Purnia	280,547
ID3	Gorakhpur	671,048
ID4	Cuttak	606,007
ID5	Lucknow	2,901,474
ID6	Kanpur	2,920,067
ID7	Bareilly	898,167
ID8	Gwalior	1,101,981
ID9	Jabalpur	1,267,564
ID10	Bhopal	1,883,381
ID11	Nagpur	2,497,777
ID12	Kota	1,001,365
ID13	Hyderabad	7,749,334

To analyze the LST and AOD level variability and to identify the interaction between the parameters, 14 biosphere reserve (BR) forests were also chosen (Table 3). A biosphere reserve forest is a protected area that prohibits human interference to conserve forest ecosystems [31].

Table 3. Selected biosphere reserves (BRs) for the study.

Code	Biosphere Reserve
BR1	Panna
BR2	Sundarban
BR3	Seshachalam
BR4	Nilgiri
BR5	Agasthyamalai
BR6	Khanchendzonga
BR7	Nokrek
BR8	Nanda Devi
BR9	Pachmarhi
BR10	Achanakmar-Amarkantak
BR11	Simlipal
BR12	Manas
BR13	Dibru-Saikhowa
BR14	Dihang-Dibang

The current secondary data from UNESCO shows that the Nokrek biosphere reserve has a 90% forest cover while the Pachmarhi and Achanakmar-Amarkantak biosphere reserves both have 63% forest cover [32–34]. The India State Forest Report 2021 [35] shows the green cover percentage of some of the urban agglomerations (Table 4).

Table 4. Green cover percentage of some of the million-plus urban agglomerations (UAs) in India.

Urban Agglomerations	Green Cover (%)
Ahmedabad	2.07
Bengaluru	6.81
Chennai	5.28
Delhi	12.61
Hyderabad	12.90
Kolkata	0.95
Mumbai	25.41

2.1. Data Sources

AOD data were extracted for the period: 2010 to 2020, from the MODIS-TERRA monthly Deep Blue Aerosol Optical Depth 550 nm product MOD08 M3 v6.1 at a spatial resolution of 111 km at the equator. The data was downloaded using Giovanni, the Goddard Earth Sciences Data and Information Services Center (GES DISC) Interactive Online Visualization, and the NASA Analysis Infrastructure tool [36,37]. The daytime pre-monsoon (March to May) LST was also extracted for the concurrent period (2010 to 2020) from the MODIS-TERRA monthly land surface temperature product MOD11C3.006 at 5.6 km at the equator also using Giovanni.

2.2. Data Mapping

ArcMap 10.4 was used for mapping urban agglomerations (UAs), industrial districts (IDs), industrial regions, and biosphere reserve (BR) forests across the study domain (India). The maps were created with the help of a georeferencing tool and digitized using point layer in ArcMap. The grid analysis and display system (GrADS), an interactive desktop tool [38], was used for mapping the time average map of LST and AOD, which was extracted as a netCDF file from Giovanni. ArcMap was used to extract the LST and AOD values of the UAs, IDs, and BRs for India through the point layer. The extracted pixel values were used to understand the spatiotemporal distribution of LST and AOD values in India's UAs, IDs, and BRs. The LST anomaly was calculated using the following calculation:

$$\text{LST of each UA for a specific year} - \text{average LST of each UA for that specific year} \quad (1)$$

The LST anomaly map was created using ArcMap and a raster calculator as follows. The time series average LST map was created, and then subtracted from each LST map (2010–2020). A point layer was generated to extract the anomaly values. The resulting LST anomaly map shows the spatial patterns of the difference between the actual and average LST values for each UA for a specific year. To comprehend the spatial distribution of LST anomalies, the LST anomaly map pinpoints areas where LST was unusually high or low compared to the average.

2.3. Data Analysis

As part of the spatiotemporal analysis, the percentage of annual change of values calculation formula is used to determine how much the values of physical parameters have changed over the past year. The calculation follows as:

$$\begin{aligned}&(((\text{Physical parameter value of subsequent year} - \text{Physical parameter value}\\&\text{of previous year})/\text{Physical parameter value of previous year}) \times 100)\end{aligned} \quad (2)$$

This normalization provides insights into the temporal variability of physical parameters. By analyzing the percentage of annual change in physical parameter values, it is possible to identify areas or regions where significant changes are occurring and to investigate the underlying causes of these changes. To analyze the variability of the parameters, point layers have been generated through ArcMap. The pixel values of specific regions have been extracted further.

For comparing two different resolution datasets AOD and LST, it is important to account for their spatial mismatch. An interpolation method was used to integrate and improve resolution for comparing two datasets in this study. In interpolation, new, ambiguous data points are added to discrete, known points. Based on this, all interpolation techniques find more similarities and correlations between close points than those that are farther apart [39,40]. As the resolution improvement process does not include real data points, there would be some accuracy estimation problems.

As the LST values did not follow a normal distribution, the non-parametric Spearmen rank-order correlation [41] was applied to find the correlation between AOD and LST. The rank correlation coefficient, abbreviated r_S, is typically written as:

$$r_S = 1 - \frac{6\sum d_i^2}{n^3 - n} \quad (3)$$

In this expression, 'n' represents the number of measurements for each of the two variates in the correlation; d_i is obtained from the difference between each pair of ranks [42]. Although correlation by rank is generally a desirable method, gradation by rank is essentially practicable in a short series [42]. One argument against rank is that it provides a theoretically less complete criterion of correspondence than a normal distribution measurement. However, the two methods provide roughly equivalent correlation values [42].

3. Results and Discussion

This study analyses the characteristics of heating events combined with AOD level variability and their relationship in different UAs, IDs, and BRs across the Indian subcontinent. The industrial regions and districts and the 14 biosphere reserves, which are remote forest areas, were chosen for this study to observe and analyze their natural and anthropogenic atmospheric processes (Figure 1, and Tables 1–3). In a large-scale scenario of urban heating and pollution domes over the Indian subcontinent, several key factors come into play: urbanization, industrialization, population growth, and geography. Rapid urbanization and the impervious areas in cities lead to warming over cities and the formation of UHIs. The presence of industries, power plants, and manufacturing units in urban areas typically contributes to air pollution. Emissions from factories, vehicles, and power generation release pollutants such as particulate matter (PM), nitrogen oxides (NO_x), sulfur dioxide (SO_2), volatile organic compounds (VOCs), and greenhouse gases (GHGs) such as carbon dioxide (CO_2). The rapid increase in the number of vehicles, especially in densely populated urban areas, leads to higher levels of air pollution. Exhaust emissions from vehicles release harmful pollutants, including fine particulate matter and nitrogen dioxide (NO_2). Agricultural practices, waste burning, and cooking methods involving solid fuels contribute to significant amounts of smoke and particulate matter, especially in rural areas. These pollutants can be transported and trapped within urban heating and pollution domes. Geographical features, including mountain ranges and wind patterns, influence the formation and persistence of pollution domes. Local weather conditions, such as calm winds or inversions, can stall pollutants within a specific region, exacerbating the situation.

3.1. Pre-Monsoon Aerosol Optical Depth (AOD)

3.1.1. Spatiotemporal Comparison of Aerosol Optical Depth (AOD) for Industrial Regions (IDs) and Biosphere Reserves (BRs)

Comparison of the AOD levels of industrial regions and protected forest areas can provide insights into the impact of industrial activities on the environment. It is important to choose industrial relatively nearby regions, districts, and biosphere reserves of India for such a comparison. The central points of 9 major industrial regions, 7 minor industrial regions, 13 IDs, and 14 BRs with forest cover were chosen to compare the AOD level of industrial regions and protected forest areas (Figure 2).

In Figure 3, the spatiotemporal variation of pre-monsoon AOD pixels indicates the changing AOD variation across the Indo-Gangetic region, Utkal, and the Andhra plain (greenish area except for the northeastern region). As the convergence zone shifts northward during the pre-monsoon season, the surface itself is also intensely heated, causing local convection associated with strong dust storms. These storms, mainly over northwestern India, yield a great deal of soil and mineral dust into the atmosphere [43]. Based on the pixel values of time average maps of AOD, it is notable that the AOD levels vary over time and across different regions in the Indian subcontinent.

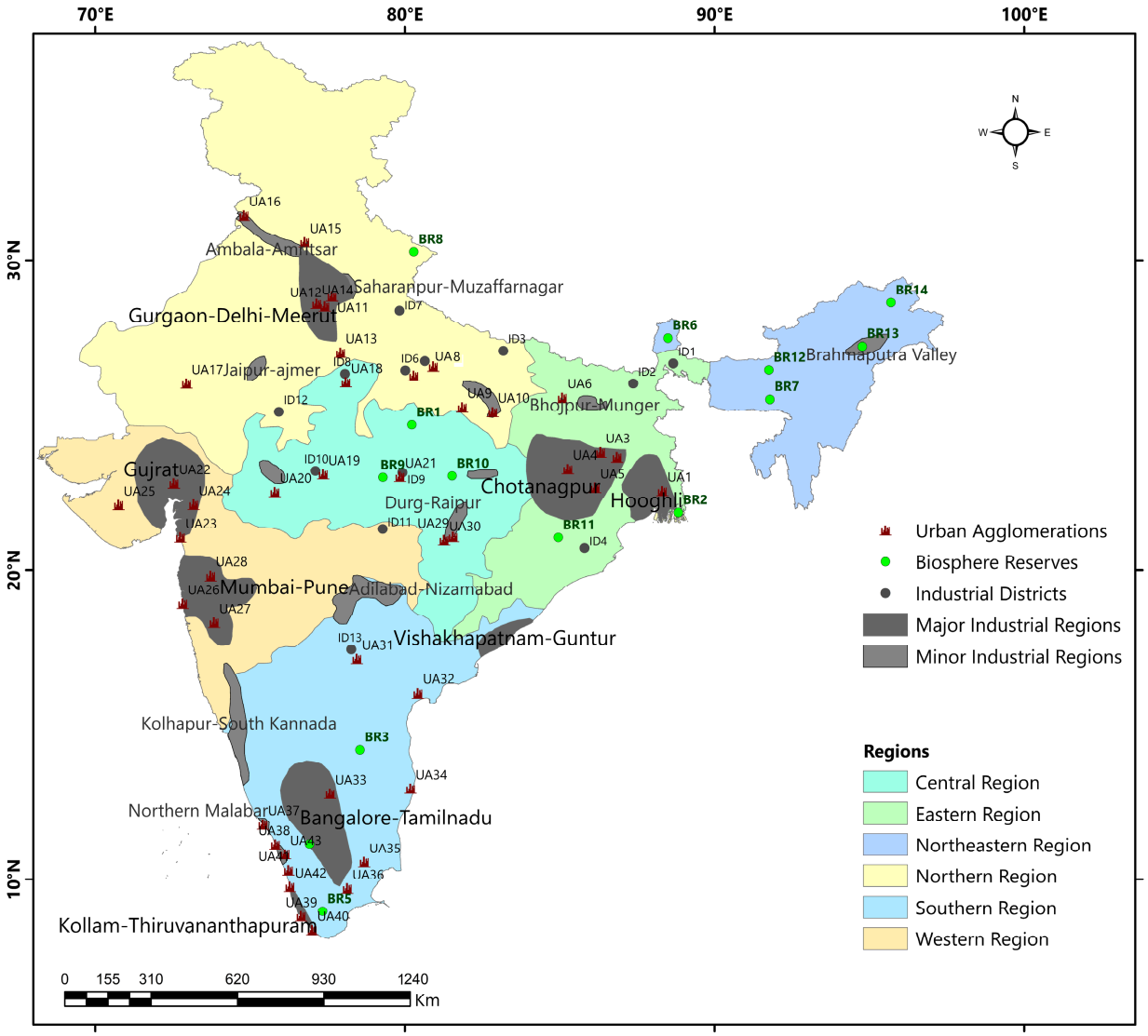

Figure 1. Urban agglomerations, (UA1) Kolkata, (UA2) Asansol, (UA3) Dhanbad, (UA4) Ranchi, (UA5) Jamshedpur, (UA6) Patna,(UA7) Lucknow, (UA8) Kanpur, (UA9) Allahabad, (UA10) Varanasi, (UA11) Meerut, (UA12) Ghaziabad, (UA13) Agra, (UA14) Delhi, (UA15) Chandigarh, (UA16) Amritsar, (UA17) Jodhpur, (UA18) Gwalior, (UA19) Bhopal, (UA20) Indore, (UA21) Jabalpur, (UA22) Ahmedabad, (UA23) Surat, (UA24) Vadodara, (UA25) Rajkot, (UA26) Mumbai, (UA27) Pune, (UA28) Nasik, (UA29) Raipur, (UA30) Durg_Bhilainagar, (UA31) Hyderabad, (UA32) Vijayawada, (UA33) Bangalore, (UA34) Chennai, (UA35) Coimbatore, (UA36) Madurai, (UA37) Kannur, (UA38) Kozhikode, (UA39) Kollam, (UA40) Thiruvananthapuram, (UA41) Thrissur, (UA42) Kochi, (UA43) Malappuram and industrial districts (ID1) Jalpaiguri, (ID2) Purnia, (ID3) Gorakhpur, (ID4) Cuttak, (ID5) Lucknow, (ID6) Kanpur, (ID7) Bareilly, (ID8) Gwalior, (ID9) Jabalpur, (ID10) Bhopal, (ID11) Nagpur, (ID12) Kota, (ID13) Hyderabadand biosphere reserves(BR1) Panna, (BR2) Sundarban, (BR3) Seshachalam, (BR4) Nilgiri, (BR5) Agasthyamalai, (BR6) Khanchendzonga, (BR7) Nokrek, (BR8) Nanda Devi, (BR9) Pachmarhi, (BR10) Achanakmar_Amarkantak, (BR11) Simlipal, (BR12) Manas, (BR13) Dibru_Saikhowa, (BR14) Dihang_Dibang in India.

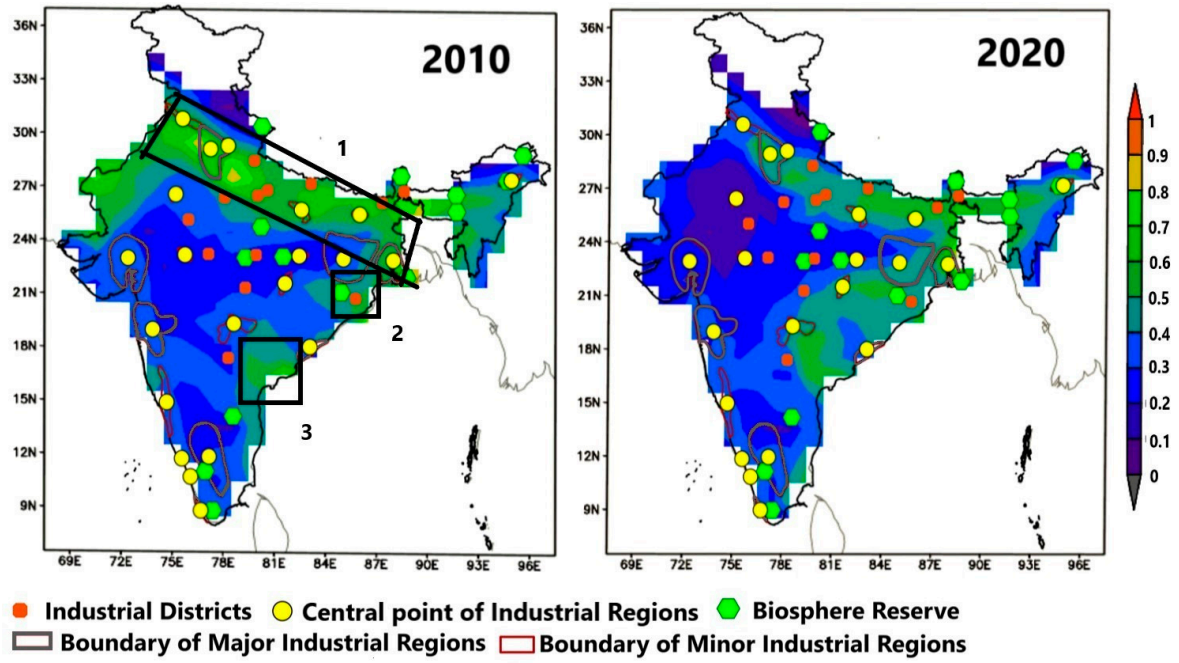

Figure 2. Locations of the selected central points of the industrial region, industrial districts, and biosphere reserve for aerosol optical depth (AOD) level analysis. Black boxes denote 1. Indo-Gangetic plain, 2. Utkal Plain, 3. Andhra Plain.

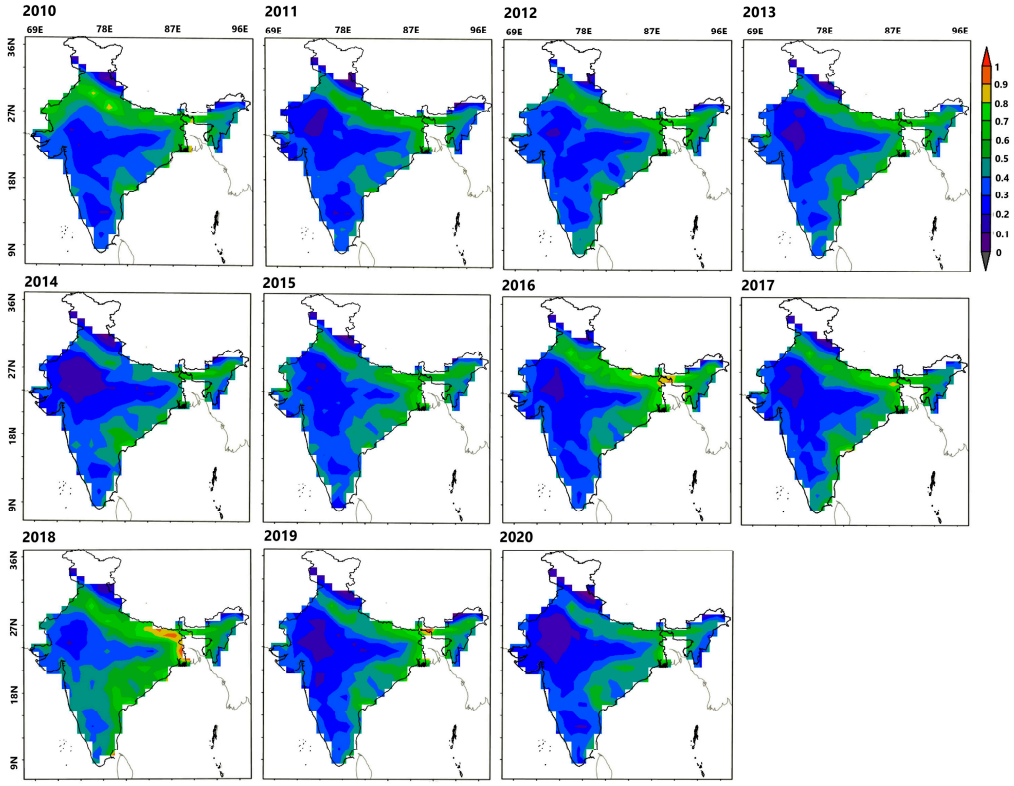

Figure 3. Time average map of pre_monsoon (March_May) aerosol optical depth (AOD) in India 2010_2020.

The Hooghli industrial region has the highest mean AOD level, followed by the Bhojpur-Munger and Allahabad-Varanasi-Mirzapur industrial regions. Specifically, the Hooghli industrial region and the Bhojpur-Munger industrial region have >0.6 AOD level on average (Figure 4). Industrial districts situated in the Indo-Gangetic plain and the eastern region of the Indian subcontinent also have higher AOD levels than other industrial districts (Figure 4). Similarly, Sundarban (BR2), Nokrek (BR7), Manas (BR12), Simlipal (BR11), and Dibru-Saikhawa (BR13) have higher AOD levels relative to other biosphere reserves. Manas has the highest mean AOD level (Figure 5).

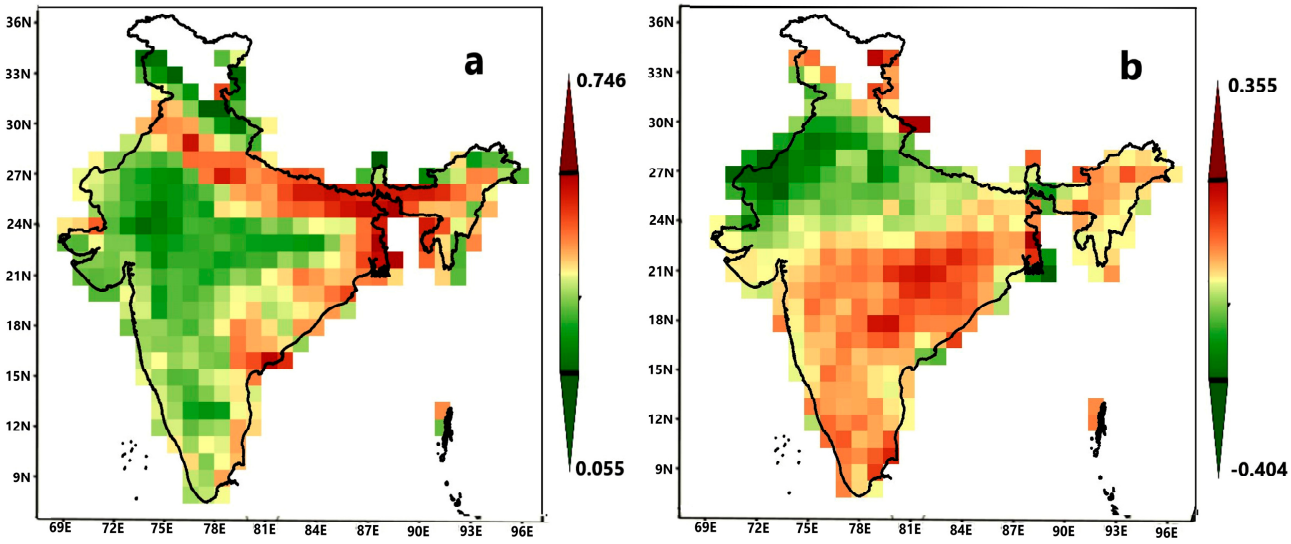

Figure 4. (**a**) Time_series average map of pre_monsoon aerosol optical depth (AOD) level (2010_2020), (**b**) pre_monsoon aerosol optical depth (AOD) difference map (2020_2010).

The AOD levels in the central area of the industrial regions and districts are generally higher than those in the nearest biosphere reserves, with the exception of the northeastern region (Figure 5). Specifically, in the Hooghli industrial region in the eastern part of the Indian subcontinent, the average pre-monsoon AOD level in the central point is 0.704, which is higher than the nearest biosphere reserve Sundarban (0.544), and the same feature is noted for the industrial district Cuttack (0.544) and the nearest biosphere reserve Simlipal (0.519).

However, in the northeastern region, the middle of the Brahmaputra valley industrial region has a lower AOD level (0.531) compared to the Dibru-Saikhowa biosphere reserve (0.534), which is also situated in the same industrial region. More in-depth study is needed to understand the reason behind such anomaly. The high AOD levels noted across India during the pre-monsoon period can have several impacts on the environment, climate, and human health. It is important to note that the impacts of pre-monsoon AOD can vary across different regions of India, depending on the sources and composition of aerosols, local weather patterns, and other factors. Monitoring and understanding these impacts are important for implementing effective air pollution control measures, climate change mitigation strategies, and public health interventions.

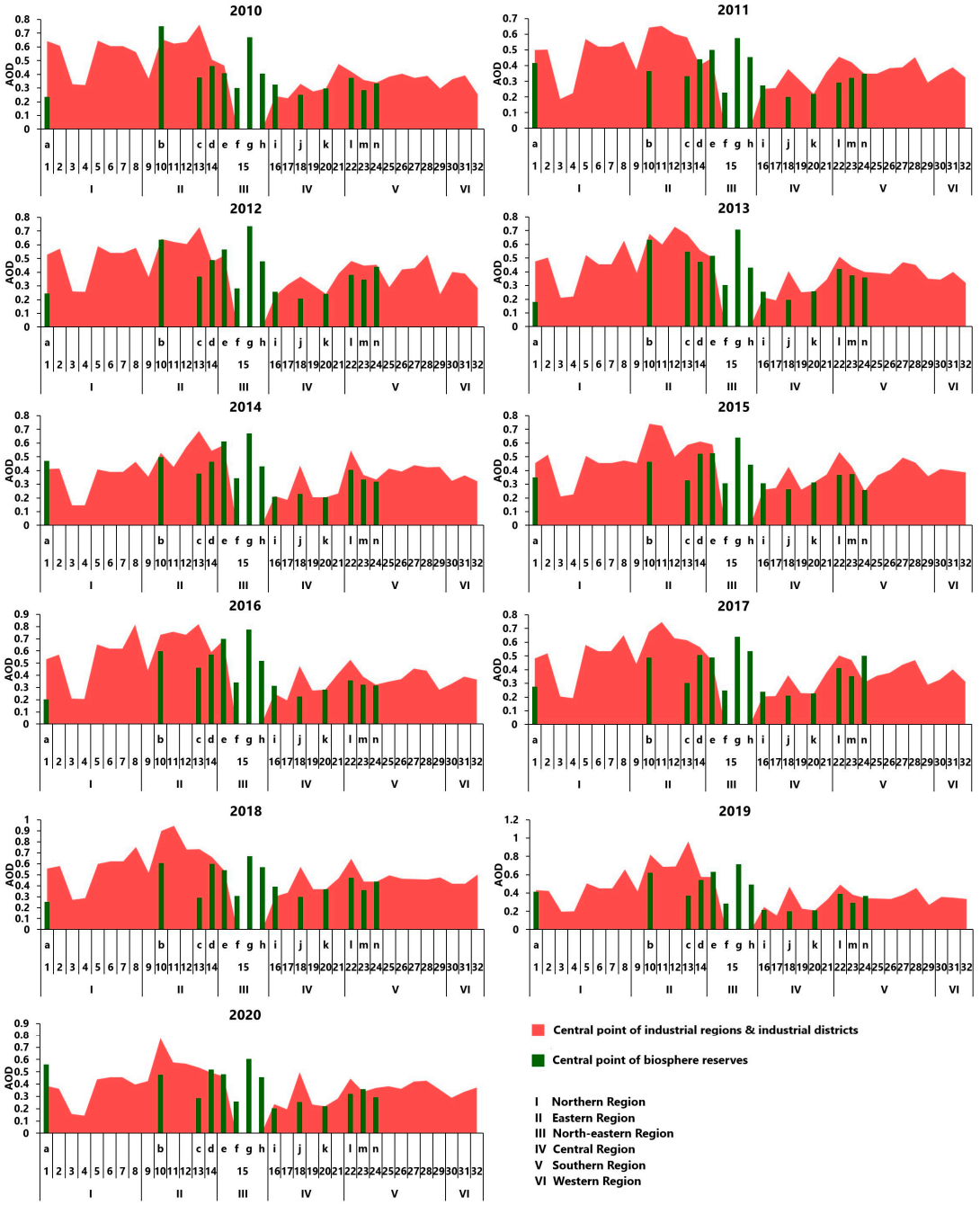

Figure 5. Spatiotemporal comparison of aerosol optical depth (AOD) level of industrial region and biosphere reserve; Respective year_wise AOD level of BRs (a) BR8, (b) BR2, (c) BR6, (d) BR11, (e) BR13, (f) BR14, (g) BR12, (h) BR7, (i) BR1, (j) BR10, (k) BR9, (l) BR3, (m) BR4, (n) BR5 and industrial regions and industrial districts (1) Gurgaon_Delhi_Meerut, (2) Ambala_Amritsar, (3) Jaipur_Ajmer, (4) ID12, (5) ID7, (6) ID6,(7) ID5, (8) ID3, (9) Chotonagpur, (10) Hooghli, (11) Bhojpur_Munger, (12) ID2, (13) ID1, (14) ID4, (15) Brahmaputra Valley, (16) Bilaspur_Korba, (17) Indore_Dewas_Ujjain, (18) Durg_Raipur, (19) ID10, (20) ID9, (21) ID8, (22) Vishakhapatnam_Guntur, (23) Bangalore_Tamilnadu, (24) Kollam_Thiruvananthapuram, (25) Adilabad_Nizamabad, (26) Kolhapur_South Kannada, (27) Northern Malabar, (28) Middle Malabar, (29) Hyderabad, (30) Gujrat, (31) Mumbai_Pune, (32) ID11.

3.1.2. Pre-Monsoon Aerosol Optical Depth (AOD) Level of Urban Agglomerations (UAs) and Industrial Districts (IDs)

Observing the AOD level of urban areas is important to understand the impact of human activities and urbanization on air pollution. The 43 UAs and 13 IDs have been analyzed further with regards to the AOD levels. The UAs and IDs were selected from different regions with varying levels of industrialization and urbanization to compare the AOD levels in these areas to identify the areas with the highest levels of air pollution.

The pixel values of time-series maps (Figure 3) indicate that Kolkata (Hooghli industrial region) has a much higher AOD (decadal average 0.708) than other UAs throughout the years due to the high concentration of AOD in the eastern portion of the Indo-Gangetic Plain (Figure 4). AOD in Kolkata (UA1) reached its maximum values in 2018 (0.899) and 2019 (0.82). The Sundarban biosphere reserve, situated in the lower Indo-Gangetic plain, about 100 km from Kolkata, had the highest pre-monsoon AOD level (0.749) in 2010, with a corresponding annual increase of 51.40%, while the AOD level decreased by 74.73% in 2012 (Table S2). AOD concentrations were typically higher in eastern and north-eastern urban areas in India, e.g., Kolkata and Cuttack (ID4), and at forest sites, e.g., the Sunderban biosphere reserve, the Simlipal biosphere reserve, the Nokrek biosphere reserve, and the Manas biosphere reserve. Marine aerosols originating from the Bay of Bengal and the emission from biomass burning in the northeastern parts of India may also have some impact on the high AOD levels there [44]. Throughout the study period (2010–2020), the urban agglomerations Patna (UA6) (Bhojpur-Munger industrial region), Allahabad (UA9), Varanasi (UA10) (Allahabad-Varanasi-Mirzapur), Meerut (UA11), Ghaziabad (UA12), and Delhi (UA14) (Gurgaon-Delhi-Meerut industrial region), and the industrial districts Kanpur (ID6), Purnia (ID2), Gorakhpur (ID3), Bareilly (ID7), all located in the Indo-Gangetic plain, also had higher AOD (decadal average > 0.54). High pre-monsoon AOD values occurred in Patna (0.873), Agra (0.734), and Varanasi (0.712) in 2018. Since 1979, the TOMS aerosol index over the Indo-Gangetic region in northern India showed an increasing trend during the pre-monsoon months (March–April–May) [45]. While transitioning from the winter season to the pre-monsoon season, the dust influx in northern India becomes more pronounced than during the winter season of dense haze and fine-particle aerosols. Dust activity typically increases during March and April and peaks in May, accompanied by severe atmospheric pollution over northern India, resulting in maximum aerosol concentration in the pre-monsoon season [45,46]. In the Utkal plain, the industrial district Cuttack has a 0.544 mean AOD level, while the nearest biosphere reserve Simlipal has a 0.510 mean AOD level. For 14 urban areas in southern India, e.g., Hyderabad (ID13), Bangalore (UA33) (Bangalore-Tamilnadu industrial region), Kannur (UA37) (Northern Malabar industrial region), Kozhikode (UA38), Thrissur (UA41), Malappuram (UA43) (Middle Malabar industrial region) Kollam (UA39), Thiruvananthapuram (UA40), Kochi (UA42) (Kollam-Thiruvananthapuram industrial region), Vijayawada (UA32), Chennai (UA34), Coimbatore (UA35), and Madurai (UA36), the mean pre-monsoonal AOD level was 0.414 in the study period (2010–2020). The highest mean AOD level was observed in Vijayawada in the Andhra plain, with a decadal average > 0.54, and the highest pre-monsoonal AOD (0.702) occurred in 2018. It appears that AOD in southern India is lower than in the north, which may be due to aerosol transport by the land-sea winds. Regarding human-produced aerosols in southern India, several factors contribute to them, including transportation and electricity production, biomass used as fuel for cooking in rural areas, crop residue burning, combustion products from small factories, and forest fires [47].

3.1.3. Pre-Monsoon Land Surface Temperatures (LSTs) in Urban Areas and Their Characteristics

In the Indian subcontinent, in the western, central, and southern parts, a particular pattern of surface heating can be identified in the spatiotemporal variations of pre-monsoon land surface temperature (Figure 6).

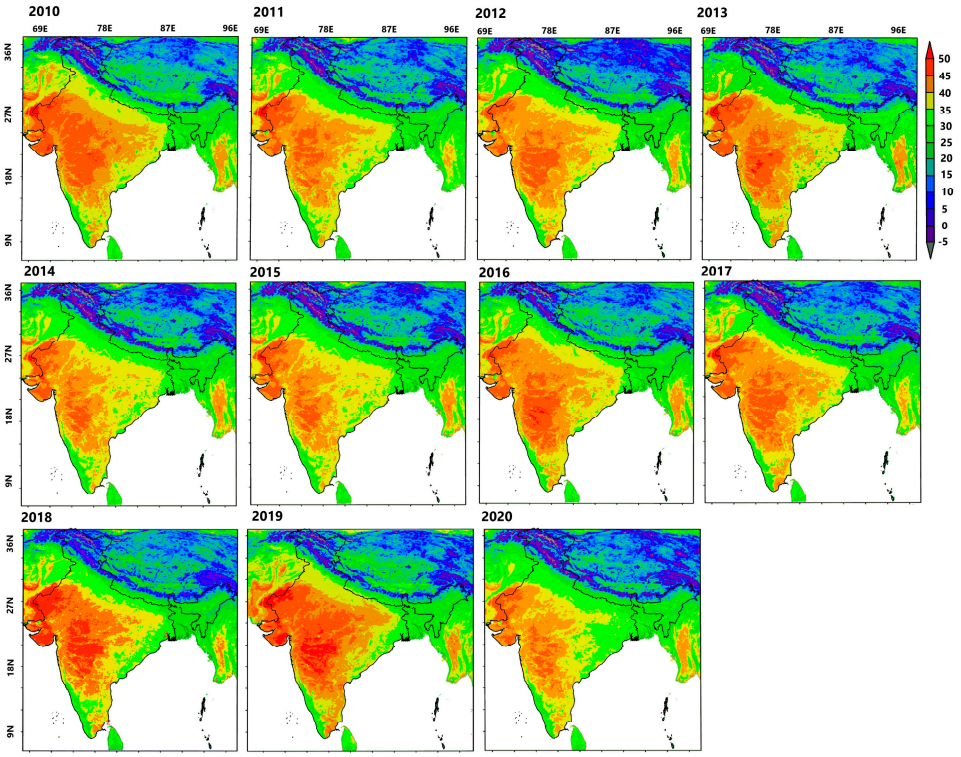

Figure 6. Time average map of pre_monsoon (March_May) land surface temperature (LST) in India 2010_2020.

Increasing temperatures in urban areas are caused mainly by lower vegetation cover, impervious surfaces, human-induced heating, and increased atmospheric pollution [48–50]. The pixel values of time series maps (Figure 6) denote that the UAs and IDs of the western part of India have an average pre-monsoon LST level of 42 °C and show the highest pre-monsoon average LST among other parts of India.

The second highest average pre-monsoon LST has been observed in the UAs and IDs of the central part of India with an average pre-monsoon LST level of 41.9 °C. Pre-monsoon LST levels in the upper southern part of India typically reach 40 °C in the UAs and IDs. Meanwhile, the UAs and IDs in the Indo-Gangetic plain experienced an average pre-monsoon LST level of 36.2 °C during the study period (2010–2020). Evaporative demand depletes the soil moisture in surrounding non-urban areas before the end of March. LSTs become much higher during April and May in India when air temperatures are also at their highest [51]. Gautam et al. [45] found that in the Indo-Gangetic plain, each pre-monsoon month displays a warming trend, but with the highest warming trend occurring in May with 2.7 °C of statistically significant warming over the three decades 1979–2009.

3.1.4. Annual Pre-Monsoon Land Surface Temperature (LST) Level Percentage Change

It appears that there have been fluctuations in pre-monsoon LST percentages among UAs and IDs in India from 2010–2020 (Figure S1, Table S3). In 2010–2011, UAs and IDs experienced an average pre-monsoon LST percentage decrease. However, this trend reversed in the following year (2011–2012) with a 75% increase in pre-monsoon LST percentages. The subsequent year (2012–2013) saw 66.07% of UAs and IDs experiencing LST increases in the pre-monsoon season. The trend then shifted back to a decrease in pre-monsoon LST percentages in 2013–2014 with a 58.93% decrease for UAs and IDs.

It is also noted that the pre-monsoon LST levels in 2020 were significantly different from the previous year, as the pre-monsoon LST in 2019 was anomalously high. The LST values notably decreased in several UAs and IDs. However, some studies observed that there was a temporary decline in land surface temperatures in certain urban areas during the COVID-19

pandemic [52,53]. For example, one study conducted in Wuhan, China, found that land surface temperatures decreased during the city's lockdown period due to reduced human activity and associated reductions in energy consumption and vehicle emissions [52]. Another study in India concluded that the lockdown measures implemented during the COVID-19 pandemic had varying impacts on reducing the mean LST of different urban agglomerations, though the magnitude of this impact has varied between urban areas due to multiple factors such as regional land use, local meteorology, and climate [53].

3.1.5. Land Surface Temperatures (LST) Anomaly Map Showing Increasing and Decreasing Trends during Pre-Monsoon (March–May) Season in India 2010–2020

The time series maps of the LST anomaly (Figure 7) denote the increasing LST anomaly in 2010 and decreasing LST anomaly in the 2020 pre-monsoon season.

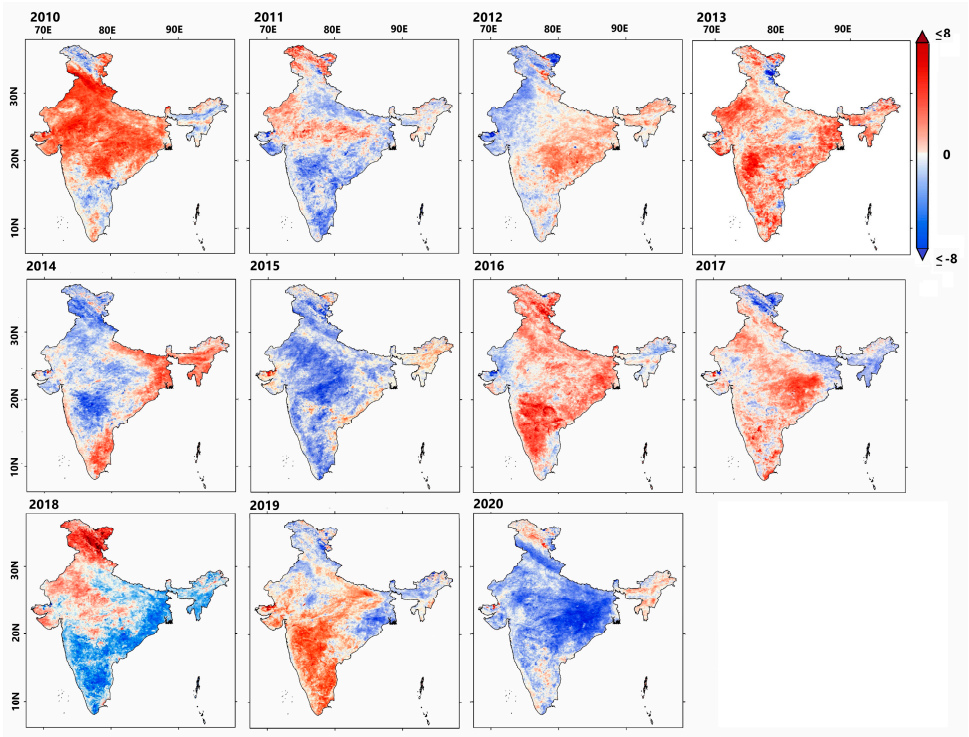

Figure 7. Land surface temperature (LST) anomaly map showing increasing and decreasing trends during pre-monsoon (March_May) season in India 2010_2020.

A decline in pre-monsoon LST anomalies had been observed in 40 UAs and IDs out of 56 UAs and IDs in 2020 (Table S4). The increasing or decreasing pattern or variable suggests that the LST level of the 56 UAs and IDs reflects the influence of many factors, such as climatological trends, geography, air quality, and level of industrial activity [53]. A decline in pre-monsoon LST anomalies had been observed in 9 out of 14 BR forests in 2020, including Pachmarhi (−3.77 °C), Panna (−2.92 °C), Agasthyamalai (−3.5 °C), Seshachalam (−4.46 °C), Dibru-Saikhowa (−0.8 °C), Dihang-Dibang (−3.21 °C), Khanchendzonga (−2.37 °C), Achanakmar-Amarkantak (−7.6 °C), and Simlipal (−0.46 °C). One exception is Sundarban (105 km from Kolkata), where no notable change was observed during the study period (2010–2020) (Table S5). Since anthropogenic activity was curbed across the country to contain the spread of COVID-19, the severity and extent of forest and nearby emissions were expected to dramatically decrease, as the vast majority of forest fires in India are due to anthropogenic activity [54]. This may affect the LST level in forests.

3.1.6. Year-Wise LST of Urban Agglomerations (UAs), Industrial Districts (IDs), and Biosphere Reserves (BRs)

Most BRs have lower pre-monsoon LST levels compared to nearby UAs and IDs (Figure 8). In the central part of India, the average pre-monsoon LST level of UAs and IDs (41.9 °C) was higher than that of BRs (41.15 °C).

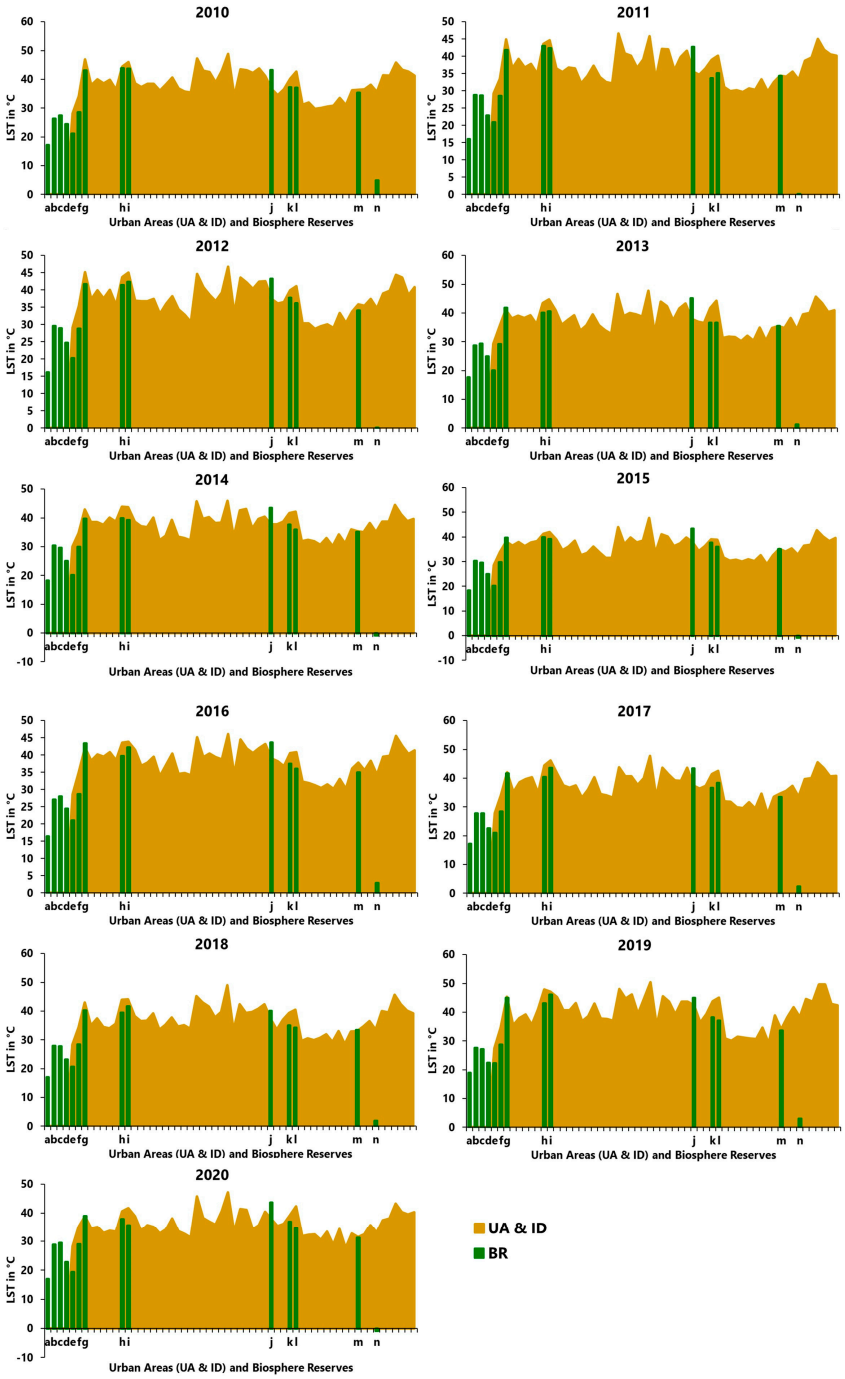

Figure 8. Year_wise corresponding land surface temperature (LST) of urban agglomerations (UAs) and industrial districts (IDs) and biosphere reserves (BRs); Respective year wise LST of UAs and IDs (ID1, UA2, UA21, UA2, UA3, UA4, UA5, UA6, UA19, UA20, UA10, UA8, UA9, UA11, UA12, UA13, UA14, UA15, UA16, UA17, UA18, UA19, UA20, UA21, UA22, UA23, UA24, UA25, UA26, UA27, UA28, UA29, UA30, UA31, UA32, UA33, UA34, UA35, UA36, UA37, UA38, UA39, UA40, UA41, UA42, UA43, ID2, ID3, ID4, ID5, ID6, ID7, ID8, ID9, ID10, ID11, ID12) and BRs (a) BR14, (b) BR15, (c) BR12, (d) BR7, (e) BR6, (f) BR2, (g) BR1, (h) BR9, (i) BR10, (j) BR3, (k) BR4, (l) BR5, (m) BR11, (n) BR8.

Similarly, in the upper southern part of India, the average pre-monsoon LST level of UAs and IDs (40.6 °C) was also higher than that of BRs (38.6 °C) in the same region. Forest-covered areas have lower LSTs relative to other land covers due to the combined effects of albedo, surface roughness, and thermal properties [55–58].

However, the Seshachalam biosphere reserve (BR3) in the upper southern part of India has the highest pre-monsoon LST level (43.3 °C) among all BRs and is also higher than the UAs and IDs in the same region (Figure 8). The high LST level of the Seshachalam biosphere reserve is possibly due to its geographic location situated in a semi-arid climate zone that has a rugged topography with steep slopes, ridges, and sparse vegetation cover [59].

The pixel values indicate that BRs have lower pre-monsoon LST levels than nearby UAs and IDs in most cases, but there were exceptions with high LST levels, such as the Seshachalam biosphere reserve. The UAs, IDs, and BRs are distinct concepts that relate to different aspects of human activity and environmental conservation. However, there can be some interactions and relationships between these three entities, which can vary based on their specific geographical context and management practices.

Within UAs, there can be variations in LST based on factors such as land use patterns, building density, vegetation cover, and surface materials. By considering the relationship between LST and IDs, it is possible to develop strategies that mitigate heat emissions, reduce the impact on local temperatures, and promote sustainable development practices that prioritize energy efficiency and environmental sustainability. BRs are often designated to promote the conservation of biodiversity and sustainable development in the face of climate resiliency. Monitoring LSTs within biosphere reserves can help assess the resilience of these areas to climate impacts. Changes in LST can provide insights into temperature trends, identify areas prone to heat stress, and guide conservation strategies to enhance the adaptive capacity of ecosystems within biosphere reserves.

UAs contribute to the formation of UHIs. The higher LSTs in urban areas can impact the microclimate within the urban agglomeration. The increased heat can affect local weather patterns, precipitation, wind patterns, and the formation of clouds. It can also influence the energy demand for cooling purposes, exacerbating the UHI and creating a feedback loop. IDs often consist of factories, power plants, and other industrial facilities that release heat as a byproduct of their operations. The waste heat generated by these activities can contribute to elevated land surface temperatures in and around industrial districts.

3.2. Pre-Monsoonal Relationship between Land Surface Temperature (LST) and Aerosol Optical Depth (AOD) in the Indian Subcontinent

As part of the spatiotemporal analysis, correlation analysis has been used. In the 56 urban agglomerations and industrial districts in the Indian subcontinent, there is a statistically significant negative relationship between AOD and LST levels in the pre-monsoon season (Figure 9, and Table 5).

Table 5. Correlation between pre-monsoon aerosol optical depth (AOD) and land surface temperature (LST) in urban agglomerations (UAs) and industrial districts (IDs).

Year	Correlation	*p*-Value
2010	−0.44	0.000633
2011	−0.63	1.99×10^{-7}
2012	−0.65	7.20×10^{-8}
2013	−0.61	5.19×10^{-7}
2014	−0.49	0.000122
2015	−0.39	0.002639
2016	−0.52	4.32×10^{-5}
2017	−0.52	4.18×10^{-5}
2018	−0.38	0.004166
2019	−0.52	3.29×10^{-5}
2020	−0.46	0.00039

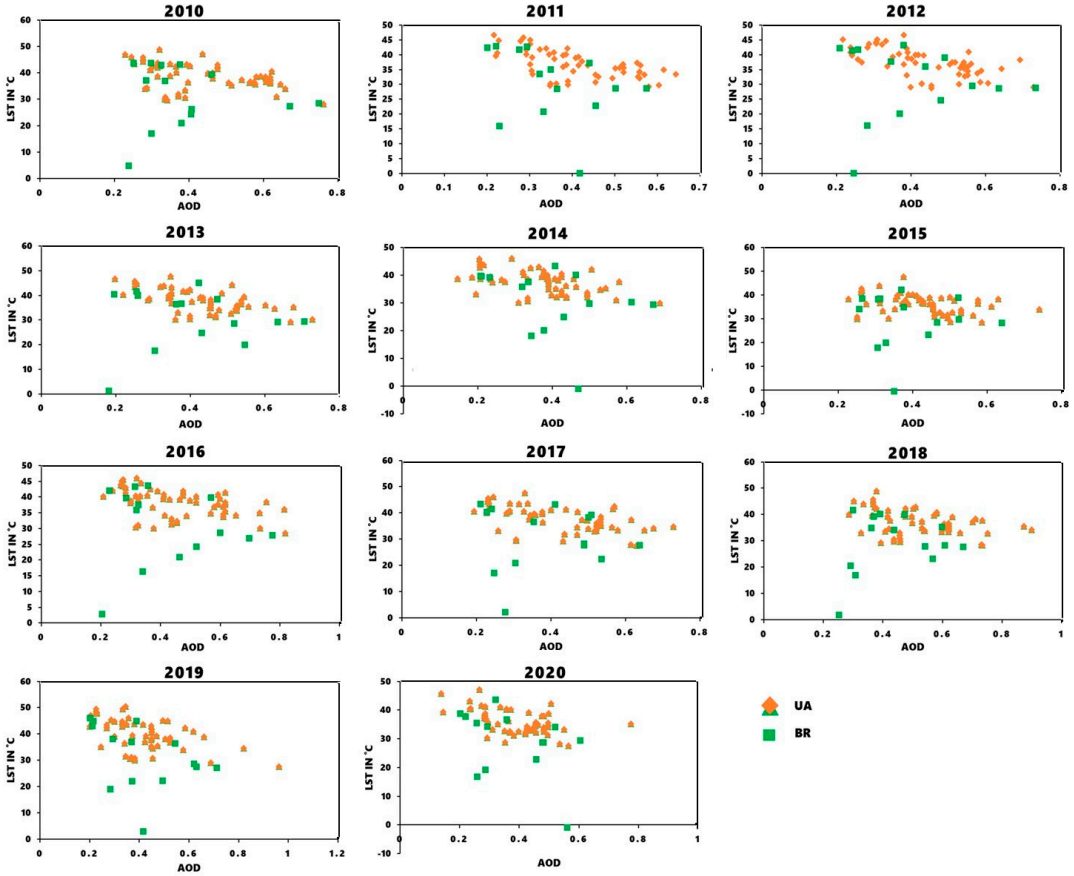

Figure 9. Scatter plot showing year_wise aerosol optical depth (AOD) and land surface temperature (LST) relationship in urban agglomerations (UAs) and biosphere reserves (BRs).

This denotes that as AOD levels increase, LST levels tend to decrease, possibly due to the solar dimming effect, as the thick layer of aerosol acts as a barrier to incoming solar radiation and can reduce surface insolation, resulting in a lower surface temperature [23,45,60]. Sen Roy [15] also observed in a study on the Indo-Gangetic plain that AOD was generally negatively related to temperature to some extent over the urban domain.

This relationship was strongest in 2012 with a correlation coefficient of −0.65 but weakened in 2018 with a coefficient of −0.38 (Table 5). However, in biosphere reserves in the Indian subcontinent, there does not appear to be a significant relationship between AOD and LST levels (Figure 9 and Table 6).

Table 6. Correlation between pre-monsoon aerosol optical depth (AOD) and land surface temperature (LST) in biosphere reserves (BRs).

Year	Correlation	*p*-Value
2010	−0.14	0.6369
2011	−0.45	0.1022
2012	−0.22	0.4549
2013	−0.19	0.5126
2014	−0.40	0.154
2015	−0.06	0.8403
2016	−0.17	0.5528
2017	−0.24	0.4001
2018	0.13	0.6696
2019	−0.48	0.08142
2020	−0.44	0.1178

This suggests that the factors influencing LST levels in BRs may be different from those in UAs and IDs.

4. Conclusions

This study used time series analysis to examine spatiotemporal variations, characteristics, and correlations between natural and anthropogenic physical parameters in urban areas. The pre-monsoonal season (March–May) data of LST and AOD of the Indian subcontinent during 2010–2020, shed light on both large-scale and regional-scale atmospheric characteristics. AOD and LST are important parameters for studying the air quality and thermal environment of a region, and they can be affected by various factors such as human activities, weather conditions, vegetation cover, and topography.

As shown by the time series analysis, the Indo-Gangetic plain, especially the eastern portion, including Kolkata had higher AOD concentrations throughout the study period (decadal average 0.708). Whereas the urban areas of the western (decadal average 42 °C), central (decadal average 41.9 °C), and southern regions (decadal average 40 °C) of the Indian subcontinent experienced the highest pre-monsoon surface heating. During the 2020 pre-monsoon season, there was a decrease (for 89% urban areas) in LSTs compared to the previous year. Urban agglomerations and industrial districts are characterized by high levels of anthropogenic activities such as transportation, industrial production, and energy consumption, which can lead to increased emissions of particulate matter and other pollutants that can affect AOD and LST levels.

An increased concentration of AOD impacts the energy budget and reduces surface temperature, as evidenced by the negative correlation (average -0.51) between pre-monsoonal time-averaged LST and AOD in UAs and IDs. The correlation analysis also pointed out that other factors can influence LST levels in BRs, and these factors may be different from those in urban and industrial areas. In contrast to the AOD and LST relationship in urban areas, biosphere reserves may have lower levels of human activity and more natural vegetation cover, which can have a moderating effect on AOD and LST levels. Additionally, topographical factors such as altitude, slope, and aspect can also influence local climate patterns and affect AOD and LST levels.

Compared to non-forested areas, forests have different thermal patterns due to the vegetation's ability to provide shade, change the microclimate, and affect the local energy balance. To fully understand the relationship between LST and AOD in forests, it is important to consider the unique features of the forest ecosystem as well as the regional environmental factors that may affect this relationship. It is significant to further study in a more detailed way these factors and their effects on mesoclimate and microclimate patterns. Other possible influencing geophysical factors can be studied to better understand them and their practical use for policymakers.

Addressing urban heating and pollution domes requires a multi-faceted approach. Implementing green building practices, incorporating green spaces, and promoting sustainable transportation systems can help mitigate the UHI effects and reduce pollution. Encouraging the adoption of renewable energy sources and improving energy efficiency can reduce the reliance on fossil fuels and lower emissions from power generation and transportation. Raising awareness about the impacts of urban heating and pollution on health and the environment is important.

This study has some notable limitations, such as the use of the point layer to derive pixel-based values of LST and AOD for selected UAs, IDs, and BRs; this method may cause some observational and analysis errors. Another limitation is the use of interpolation algorithms for image enhancement; this estimates the values of missing pixels based on the pixels around them, and this estimation process can cause errors and distortions in the image. These errors and distortions may affect the correlation result slightly. The large-scale observations of this study serve as preliminary work before looking at the physics and chemistry behind the combined variations of atmospheric parameters on smaller scales in mesoclimates and microclimates.

Supplementary Materials: The following supporting information can be downloaded at: https://www.mdpi.com/article/10.3390/rs15102681/s1, Table S1. Annual pre-monsoon AOD level percentage change of 43 urban agglomerations and 13 industrial districts. Table S2. Annual pre-monsoon AOD level percentage change of 14 biosphere reserves. Table S3. Annual pre-monsoon LST level percentage change of 43 urban agglomerations and 13 industrial districts. Table S4. LST anomaly of pre-monsoon average LST of 43 urban agglomerations and 13 industrial districts. Table S5. LST anomaly of pre-monsoon average LST of 14 biosphere reserves. Figure S1. Annual pre-monsoon LST level percentage change.

Author Contributions: T.C.: Conceptualization, methodology, software, validation, and formal analysis, resources, data curation, writing—original draft preparation, writing—review and editing, visualization; D.D.: Conceptualization, writing—review, visualization, supervision; R.H.: Writing—review, visualization, supervision; A.K.: Conceptualization, writing—review, visualization, supervision; D.N.: Conceptualization, writing—review, supervision. All authors have read and agreed to the published version of the manuscript.

Funding: T.C. would like to express her gratitude to the UGC Junior Research Fellowship (India), grant number UGC-Ref No.: 3421/(NET-DEC 2018), for funding this research. D.N. acknowledges the William Stamps Farish Chair endowments at the University of Texas at Austin.

Data Availability Statement: Data used in this paper are open source; they can be downloaded from the official site https://giovanni.gsfc.nasa.gov/giovanni/ (accessed on 8 December 2022) without any charges. More information about the results and analysis is available on reasonable request to the corresponding author.

Acknowledgments: T.C. and D.D. would like to thank the Department of Architecture of Jadavpur University, Kolkata for providing the laboratory and computational facilities for the study.

Conflicts of Interest: The authors declare no conflict of interest.

References

1. Crutzen, P.J. New Directions: The growing urban heat and pollution "island" effect—Impact on chemistry and climate. *Atmos. Environ.* **2004**, *38*, 3539–3540. [CrossRef]
2. Balakrishnan, K.; Dey, S.; Gupta, T.; Dhaliwal, R.S.; Brauer, M.; Cohen, A.J.; Stanaway, J.D.; Beig, G.; Joshi, T.K.; Aggarwal, A.N.; et al. The impact of air pollution on deaths, disease burden, and life expectancy across the states of India: The Global Burden of Disease Study 2017. *Lancet Planet. Health* **2019**, *3*, e26–e39. [CrossRef] [PubMed]
3. Khan, A.; Khorat, S.; Khatun, R.; VanDoan, Q.; Nair, U.S.; Niyogi, D. Variable impact of COVID-19 lockdown on air quality across 91 Indian cities. *Earth Interact.* **2021**, *25*, 57–75. [CrossRef]
4. Global Burden of Disease Collaborative Network. *Global Burden of Disease Study 2016 (GBD 2016)*; Institute for Health Metrics and Evaluation (IHME): Seattle, WA, USA, 2017.
5. Ramanathan, V.; Crutzen, P.J.; Kiehl, J.T.; Rosenfeld, D. Atmosphere: Aerosols, climate, and the hydrological cycle. *Science* **2001**, *294*, 2119–2124. [CrossRef]
6. Wang, H.; Shi, G.Y.; Zhang, X.Y.; Gong, S.L.; Tan, S.C.; Chen, B.; Che, H.Z.; Li, T. Mesoscale modeling study of the interactions between aerosols and PBL meteorology during a haze episode in China Jing-Jin-Ji and its near surrounding region-Part 2: Aerosols' radiative feedback effects. *Atmos. Chem. Phys. Discuss.* **2014**, *14*, 28269–28298. [CrossRef]
7. Wang, Z.; Lin, L.; Yang, M.; Guo, Z. The Role of Anthropogenic Aerosol Forcing in Interdecadal Variations of Summertime Upper-Tropospheric Temperature Over East Asia. *Earth's Future* **2019**, *7*, 136–150. [CrossRef]
8. Das, S.; Giorgi, F.; Giuliani, G.; Dey, S.; Coppola, E. Near-Future Anthropogenic Aerosol Emission Scenarios and Their Direct Radiative Effects on the Present-Day Characteristics of the Indian Summer Monsoon. *J. Geophys. Res. Atmos.* **2020**, *125*, e2019JD031414. [CrossRef]
9. Grey, I.; Arora, T.; Thomas, J.; Saneh, A.; Tohme, P.; Abi-habib, R. Since January 2020 Elsevier has created a COVID-19 resource centre with free information in English and Mandarin on the novel coronavirus COVID-19. The COVID-19 resource centre is hosted on Elsevier Connect, the company' s public news and information. *Psychiatry Res.* **2020**, *14*, 293.
10. Merikanto, J.; Nordling, K.; Räisänen, P.; Räisänen, J.; O'donnell, D.; Partanen, A.I.; Korhonen, H. How Asian aerosols impact regional surface temperatures across the globe. *Atmos. Chem. Phys.* **2021**, *21*, 5865–5881. [CrossRef]
11. Kumar, R.; Barth, M.C.; Pfister, G.G.; Naja, M.; Brasseur, G.P. WRF-Chem simulations of a typical pre-monsoon dust storm in northern India: Influences on aerosol optical properties and radiation budget. *Atmos. Chem. Phys.* **2014**, *14*, 2431–2446. [CrossRef]
12. Ginoux, P.; Prospero, J.M.; Gill, T.E.; Hsu, N.C.; Zhao, M. Global-scale attribution of anthropogenic and natural dust sources and their emission rates based on MODIS Deep Blue aerosol products. *Rev. Geophys.* **2012**, *50*, 1–36. [CrossRef]
13. Prasad, A.K.; Singh, S.; Chauhan, S.S.; Srivastava, M.K.; Singh, R.P.; Singh, R. Aerosol radiative forcing over the Indo-Gangetic plains during major dust storms. *Atmos. Environ.* **2007**, *41*, 6289–6301. [CrossRef]

14. Pan, X.; Chin, M.; Gautam, R.; Bian, H.; Kim, D.; Colarco, P.R.; Diehl, T.L.; Takemura, T.; Pozzoli, L.; Tsigaridis, K.; et al. A multi-model evaluation of aerosols over South Asia: Common problems and possible causes. *Atmos. Chem. Phys.* **2015**, *15*, 5903–5928. [CrossRef]
15. Roy, S.S. Impact of aerosol optical depth on seasonal temperatures in India: A spatio-temporal analysis. *Int. J. Remote Sens.* **2008**, *29*, 727–740. [CrossRef]
16. Kothawale, D.R.; Revadekar, J.V.; Kumar, K.R. Recent trends in pre-monsoon daily temperature extremes over India. *J. Earth Syst. Sci.* **2010**, *119*, 51–65. [CrossRef]
17. Available online: https://mausam.imd.gov.in/imd_latest/contents/ar2020.pdf (accessed on 25 May 2022).
18. Keramitsoglou, I.; Daglis, I.A.; Amiridis, V.; Chrysoulakis, N.; Ceriola, G.; Manunta, P.; Maiheu, B.; De Ridder, K.; Lauwaet, D.; Paganini, M. Evaluation of satellite-derived products for the characterization of the urban thermal environment. *J. Appl. Remote Sens.* **2012**, *6*, 061704. [CrossRef]
19. Chakraborty, K.; Raju, P.L.N. Remote sensing technique-a tool for environmental studies. *ADBU J. Eng. Technol. Chakraborty* **2017**, *6*, 1–6.
20. Pandey, P.; Kumar, D.; Prakash, A.; Kumar, K.; Jain, V.K. A Study of the Summertime Urban Heat Island over Delhi. *Int. J. Sustain. Sci. Stud.* **2009**, *1*, 27–34.
21. Li, H.; Meier, F.; Lee, X.; Chakraborty, T.; Liu, J.; Schaap, M.; Sodoudi, S. Interaction between Urban Heat Island and Urban Pollution Island during Summer in Berlin. *Sci. Total Environ.* **2018**, *636*, 818–828. [CrossRef]
22. Sussman, H.S.; Ajay Raghavendra, A.; Zhou, L. Impacts of increased urbanization on surface temperature, vegetation, and aerosols over Bengaluru, India. *Remote Sens. Appl. Soc. Environ.* **2019**, *16*, 100261. [CrossRef]
23. Sarthi, P.P.; Kumar, S.; Barat, A.; Kumar, P.; Sinha, A.K.; Goswami, V. Linkage of Aerosol Optical Depth with Rainfall and Circulation Parameters over the Eastern Gangetic Plains of India. *J. Earth Syst. Sci.* **2019**, *128*, 171. [CrossRef]
24. Han, W.; Li, Z.; Wu, F.; Zhang, Y.; Guo, J.; Su, T.; Cribb, M.; Fan, J.; Chen, T.; Wei, J.; et al. The Mechanisms and Seasonal Differences of the Impact of Aerosols on Daytime Surface Urban Heat Island Effect. *Atmos. Chem. Phys.* **2020**, *20*, 6479–6493. [CrossRef]
25. AlFaisal, A.; Rahman, M.M.; Haque, S. Retrieving Spatial Variation of Aerosol Level over Urban Mixed Land Surfaces Using Landsat Imageries: Degree of Air Pollution in Dhaka Metropolitan Area. *Phys. Chem. Earth* **2022**, *126*, 103074. [CrossRef]
26. Mal, S.; Rani, S.; Maharana, P. Estimation of Spatio-Temporal Variability in Land Surface Temperature over the Ganga River Basin Using MODIS Data. *Geocarto Int.* **2022**, *37*, 3817–3839. [CrossRef]
27. Mielonen, T.; Hienola, A.; Merikanto, J.; Lipponen, A.; Laakso, A.; Bergman, T.; Korhonen, H.; Kolmonen, P.; Ghent, D.; Arola, A.; et al. The Climatic Significance of Biogenic Aerosols in the Boreal Region Now and in the Future. *Authorea Prepr.* **2018**, 5–6. [CrossRef]
28. Census 2021-Formation of Urban Agglomerations.pdf. Available online: https://censusindia.gov.in/nada/index.php/catalog/40512/download/44144/ORGI_circular003_2021.pdf (accessed on 1 January 2023).
29. Putnik, D.G.; Cruz-Cunha, M.M. *Encyclopedia of Networked and Virtual Organizations (3 Volumes)*; IGI Global: Hershey, PA, USA, 2008. [CrossRef]
30. Available online: https://msme.gov.in/ (accessed on 1 January 2022).
31. Available online: https://en.unesco.org/biosphere/about/ (accessed on 1 January 2023).
32. Available online: https://en.unesco.org/biosphere/aspac/nokrek (accessed on 28 April 2023).
33. Available online: https://en.unesco.org/biosphere/aspac/pachmarhi (accessed on 28 April 2023).
34. Available online: https://en.unesco.org/biosphere/aspac/achanakmar-amarkantak (accessed on 28 April 2023).
35. Available online: https://fsi.nic.in/forest-report-2021-details (accessed on 28 April 2023).
36. Acker, J.G.; Leptoukh, G. Online analysis enhances use of NASA Earth Science Data. *Eos Trans. Am. Geophys. Union* **2007**, *88*, 14–17. [CrossRef]
37. Available online: https://giovanni.gsfc.nasa.gov/giovanni/ (accessed on 20 May 2022).
38. Available online: http://cola.gmu.edu/grads/ (accessed on 2 March 2022).
39. Aftab, H.; Mansoor, A.B.; Asim, M. A New Single Image Interpolation Technique for Super Resolution. In Proceedings of the 2008 IEEE International Multitopic Conference, Karachi, Pakistan, 23–24 December 2008; pp. 592–596. [CrossRef]
40. Setianto, A.; Triandini, T. Comparison of Kriging and Inverse Distance Weighted (Idw) Interpolation Methods in Lineament Extraction and Analysis. *J. Appl. Geol.* **2015**, *5*, 21–29. [CrossRef]
41. Spearman, C. The Proof and Measurement of Association between Two Things. *Am. J. Psychol.* **1904**, *15*, 72–101. [CrossRef]
42. Zar, J.H. Significance Testing of the Spearman Rank Correlation Coefficient. *J. Am. Stat. Assoc.* **1972**, *67*, 578–580. [CrossRef]
43. Acharya, P.; Sreekesh, S. Seasonal variability in aerosol optical depth over India: A spatio-temporal analysis using the MODIS aerosol product. *Int. J. Remote Sens.* **2013**, *34*, 4832–4849. [CrossRef]
44. Singh, N.; Mhawish, A.; Deboudt, K.; Singh, R.S.; Banerjee, T. Organic aerosols over Indo-Gangetic Plain: Sources, distributions and climatic implications. *Atmos. Environ.* **2017**, *157*, 59–74. [CrossRef]
45. Gautam, R.; Hsu, N.C.; Lau, K.M.; Tsay, S.C.; Kafatos, M. Enhanced pre-monsoon warming over the Himalayan-Gangetic region from 1979 to 2007. *Geophys. Res. Lett.* **2009**, *36*, 1–5. [CrossRef]
46. Gautam, R.; Hsu, N.C.; Tsay, S.C.; Lau, K.M.; Holben, B.; Bell, S.; Smirnov, A.; Li, C.; Hansell, R.; Ji, Q.; et al. Accumulation of aerosols over the Indo-Gangetic plains and southern slopes of the Himalayas: Distribution, properties and radiative effects during the 2009 pre-monsoon season. *Atmos. Chem. Phys.* **2011**, *11*, 12841–12863. [CrossRef]

47. Dey, S.; Rongali, G. Aerosol Climatology and Intercomparison. In *Satellite Meteoreology and Remote Sensing*; Indian Institute of Technology: Delhi, India, 2014; pp. 1–17. Available online: https://web.iitd.ac.in/~sagnik/SN1.pdf (accessed on 2 January 2023).
48. Grimmond, S. Urbanization and global environmental change: Local effects of urban warming. *Geogr. J.* **2007**, *173*, 83–88. [CrossRef]
49. Grimmond, C.S.B.; Ward, H.C.; Kotthaus, S. How is urbanization altering local and regional climate? In *The Routledge Handbook of Urbanization and Global Environmental Change*; Routledge: New York, NY, USA, 2016; pp. 1–10.
50. Hamdi, R.; Kusaka, H.; Van Doan, Q.; Cai, P.; He, H.; Luo, G.; Kuang, W.; Caluwaerts, S.; Duchêne, F.; Van Schaeybroek, B.; et al. The State-of-the-Art of Urban Climate Change Modeling and Observations. *Earth Syst. Environ.* **2020**, *4*, 631–646. [CrossRef]
51. Kumar, R.; Mishra, V.; Buzan, J.; Kumar, R.; Shindell, D.; Huber, M. Dominant control of agriculture and irrigation on urban heat island in India. *Sci. Rep.* **2017**, *7*, 14054. [CrossRef]
52. Hadibasyir, H.Z.; Rijal, S.S.; Sari, D.R. Comparison of Land Surface Temperature During and Before the Emergence of Covid-19 using Modis Imagery in Wuhan City, China. *Forum Geogr.* **2020**, *34*, 1–15. [CrossRef]
53. Nanda, D.; Mishra, D.R.; Swain, D. COVID-19 lockdowns induced land surface temperature variability in mega urban agglomerations in India. *Environ. Sci. Processes Impacts* **2021**, *23*, 144–159. [CrossRef]
54. Gupta, A.; Bhatt, C.M.; Roy, A.; Chauhan, P. COVID-19 Lockdown a Window of Opportunity to Understand the Role of Human Activity on Forest Fire Incidences in the Western Himalaya, India. *Curr. Sci.* **2020**, *119*, 390. [CrossRef]
55. Bala, G.; Caldeira, K.; Wickett, M.; Phillips, T.J.; Lobell, D.B.; Delire, C.; Mirin, A. Combined Climate and Carbon-Cycle Effects of Large-Scale Deforestation. *Proc. Natl. Acad. Sci. USA* **2007**, *104*, 6550–6555. [CrossRef]
56. Betts, R.A. Offset of the Potential Carbon Sink from Boreal Forestation by Decreases in Surface Albedo. *Nature* **2000**, *408*, 187–190. [CrossRef] [PubMed]
57. Marland, G.; Pielke, R.A.; Apps, M.; Avissar, R.; Betts, R.A.; Davis, K.J.; Frumhoff, P.C.; Jackson, S.T.; Joyce, L.A.; Kauppi, P.; et al. The Climatic Impacts of Land Surface Change and Carbon Management, and the Implications for Climate-Change Mitigation Policy. *Clim. Policy* **2003**, *3*, 149–157. [CrossRef]
58. Peng, S.; Piao, S.; Zeng, Z.; Ciais, P.; Zhou, L.; Li, L.Z.X.; Myneni, R.B. Afforestation in China Cools Local Land Surface Temperature. *Proc. Natl. Acad. Sci. USA* **2014**, *111*, 2915–2919. [CrossRef] [PubMed]
59. Available online: https://www.britannica.com/place/Seshachalam-Hills/ (accessed on 3 March 2023).
60. Jin, M.; Shepherd, J.M.; Zheng, W. Urban Surface Temperature Reduction via the Urban Aerosol Direct Effect: A Remote Sensing and WRF Model Sensitivity Study. *Adv. Meteorol.* **2010**, *2010*, 681587. [CrossRef]